Large Strain With Ultra-Low Hysteresis and Enhanced Energy Storage Performance of Mn-Doped 0.65Bi0.5Na0.5TiO3-0.35SrTiO3 Lead-Free Ceramics

W.P. Cao (xiao5460hu@126.com)
Harbin University of Commerce
Weili Li
Harbin Institute of Technology
Wenzhong Zhang
Harbin Institute of Technology
Dan Xu
Harbin University of Science and Technology
Jie Sheng
Harbin Institute of Technology

Research Article

Keywords: NBT-based ceramics, defect dipoles, electric-field induced strain, energy storage properties, electrostrictive effect

Posted Date: February 12th, 2021

DOI: https://doi.org/10.21203/rs.3.rs-184913/v1

Large strain with ultra-low hysteresis and enhanced energy storage performance of Mn-doped $0.65Bi_{0.5}Na_{0.5}TiO_3$-$0.35SrTiO_3$ lead-free ceramics

Wenping Cao[a*], Weili Li[b], Wenzhong Zhang[b], Dan Xu[c], Jie Sheng[d]

[a] *School of Light Industry, Harbin University of Commerce, Harbin 150028, P. R. China*
[b] *School of Materials Science and Engineering, Harbin Institute of Technology, Harbin 150001, P. R. China.*
[c] *The Key Laboratory of Quantum Manipulation & Control of Heilongjiang Province, Harbin University of Science and Technology, Harbin 150080, P.R. China*
[d] *Laboratory for Space Environment and Physical Science, Research Center of Basic Space Science, Harbin Institute of Technology, Harbin 150001, PR China*

Abstract: In this paper, the electric-field-induced strain behavior and energy storage performance of MnO-doped $0.65Bi_{0.5}Na_{0.5}TiO_3$-$0.35SrTiO_3$ (NBT-ST-*x*Mn) lead-free ceramics has been investigated. After the introduction of MnO into NBT-ST ceramics, pinched and double *P*-*E* hysteresis loops with high P_{max} and negligible P_r can be observed due to the introduction of defect dipoles. As a result, a relatively high strain of 0.22% with ultra-low hysteresis of 14% was achieved under a moderate electric field of 60 kV/cm at *x*=1.0 mol.%. Excellent energy storage performance of 1.14 and 1.17 J cm^{-3} with a high η of 83 and 80% are achieved at *x*=0.5 and 1.0 mol.%, respectively. Meanwhile, high electrostriction coeffcient of 0.022 m^4C^2 with pure electrostrictive characteristics was obtained at *x*=0.5 mol.%. The results illustrate that the proper selection of base composition and effective chemical modifier can made the NBT-ST an outstanding candidate for actuators and energy storage devices.

Keywords: NBT-based ceramics; defect dipoles; electric-field induced strain; energy storage properties; electrostrictive effect

* Corresponding author: School of Light Industry, Harbin University of Commerce, Harbin 150028, P. R. China
E-mail addresses: xiao5460hu@126.com (W.P. Cao)

1 Introduction

Piezoelectric ceramics are widely applied in industrial devices such as actuators, sensors and energy storage capacitors because of their excellent electromechanical properties [1-8]. Currently, the lead-based systems, such as $Pb(Zr,Ti)O_3$ (PZT) still dominated the global piezoelectric ceramics market due to their outstanding piezoelectric properties and thermal stability [1,6]. However, lead-based materials contain much lead oxide, which is harm to the environment and human beings. Therefore, it is very necessary to seek lead-free ceramics with excellent performance to replace lead-containing materials.

Among reported lead-free ceramic systems, $Na_{0.5}Bi_{0.5}TiO_3$ (abbreviated as NBT)-based ceramics present giant electric-field induced strain [9-22], which makes NBT-based ceramics to be one of the most promising candidates to replace lead-containing materials. For example, large electric-field-induced strain value of 0.45% was achieved in $Na_{0.5}Bi_{0.5}TiO_3$-$BaTiO_3$-$K_{0.5}Na_{0.5}NbO_3$ (NBT-BT-KNN) ceramic [10]. Liu et al. [13] found that the introduction of Nb into the $Na_{0.5}Bi_{0.5}TiO_3$-$K_{0.5}Bi_{0.5}TiO_3$-$SrTiO_3$ (NBT-KBT-ST) system could induce a giant strain as high as 0.70%. The obtained large strain in NBT-based ceramics is usually attributed to the ferroelectric to relaxor phase transition induced by external electric field. Although a high strain could be obtained in BNT-based ceramics, their strain loops show serious hysteresis behavior (> 50%) with a strong nonlinearity. Therefore, how to reduce the hysteresis of NBT-based materials is a great challenge for the applications in high precision positioning devices and other actuators.

In recent years, some efforts have been devoted to reduce the hysteresis of NBT-based materials [23-34]. Ullah et al. [23] tailored the hysteresis behavior as low as 40% in Nb-doped NBT-KBT-$Ba_{0.7}Sr_{0.3}TiO_3$ (BNT-BKT-BST) ceramic. Li et al. [25] found the introduction of A-site vacancies (V_A) and oxygen vacancies (V_O) into NBT-KBT-$Sr_{0.8}Bi_{0.1}\square_{0.1}Ti_{0.8}Zr_{0.2}O_{2.95}$ system could be beneficial for the reduction of strain hysteresis. The design of ceramic/ceramic composite consisting of an ergodic relaxor (matrix) and a nonergodic or ferroelectric phase (seed) was also identified as

typical feature that could reduce the strain hysteresis [28-30]. In our previous work, both of the strain value and the hysteresis of NBT-BT-ST and NBT-ST systems could be improved simultaneously by the introducing of defect dipoles [26,34]. High strain of 0.24% under 80 kV/cm with ultra-low hysteresis (about 10%) was obtained in Mn-doped NBT-BT-ST system while large strain of 0.32% with small hysteresis of 28% was realized at 60 kV/cm in Mn-doped 0.7NBT-0.3ST system. However, the applied electric field in Mn-doped NBT-BT-ST system was too high and the strain hysteresis in Mn-doped 0.7NBT-0.3ST system was still not small enough. It is well-known that both the proper selection of base composition and effective chemical modifier doping are important to obtain excellent strain properties. Here, in order to obtain large strain under low electric field meanwhile maintain ultra-low hysteresis, we selected 0.65NBT-0.35ST ceramic as base composition which exhibits slimmer *P*-*E* loops than 0.7NBT-0.3ST ceramic, and doped with different content of MnO to achieve optimized strain properties. Meanwhile, the energy storage properties of Mn-doped 0.65NBT-0.35ST ceramic can also be enhanced due to the combined contribution of high electric breakdown feld (BDS) and P_{max}-P_r value. The influence of MnO enhancement on electric-field-induced strain and energy storage density of 0.65NBT-0.35ST ceramics were studied in details.

2 Experimental

$0.65Na_{0.5}Bi_{0.5}TiO_3$-$0.35SrTiO_3$ ceramics doped with 0, 0.5, 1 and 1.5 mol. % MnO (denoted as NBT-ST-*x*Mn) were prepared using a conventional solid-state reaction method. The raw materials of this experiment were Na_2CO_3(99.8%), Bi_2O_3(99.9%), MnO(99.5%), $SrCO_3$(99.95%) and TiO_2(99.9%). The details of sample preparation are reported elsewhere [26].

The crystal structure of sintered ceramics was analyzed using X-ray diffraction (XRD) on a Philips X'Pert diffractometer with Cu Ka radiation. The surface microstructure of the samples was observed with a scanning electron microscopy (SEM, Quanta 600F). Before electrical performance characterization, all samples were carefully ground to smooth and flat on both sides. Silver paste was first

uniformly painted onto both surfaces of each sample, and then insulated at 600°C for 40 min to form electrodes. The dielectric constant and dielectric loss as a function of temperature (30-400°C) were carried out using an Agilent 4294A precision impedance analyzer with the discrete frequencies: 1 kHz, 10 kHz and 100 kHz. Ferroelectric hysteresis loops (*P-E*) and electrostrain curves (*S-E*) were measured using a Radiant Technologies Precision II (Radiant Tech.USA) in a silicone oil bath.

3 Results and discussion

X-ray diffraction patterns of the NBT-ST-*x*Mn ceramics are displayed in Fig. 1. As shown in Fig. 1(a), all samples exhibited a single phase perovskite structure without apparent secondary phases, which proved that the MnO had completely incorporated into the structure of the 0.65NBT-0.35ST ceramics. The characterization of (200) peaks of the four samples was investigated in detail to obtain the phase structure evolution, as shown in Fig. 1(b). Obvious splitting of (002) and (200) peaks were detected between 44° and 48° for all the samples, indicating a tetragonal distortion of the pseudocubic lattice.

Fig. 2 shows the surface microstructure images (SEM) of NBT-ST-*x*Mn ceramics with different Mn doping levers. Nearly no pores were observed on the images of all the samples, suggesting that the ceramics were densely sintered. For the sample with *x*=0.0 mol.%, the average grain size is about 2 μm. After doping with a slight amount of MnO, the grain size increases obviously, and both of the large and small grains can be observed in the same sample. With the further increase of *x*, the grains further grow up and the proportion of large ones obviously increase. The maximum grain size can reach to about 20 μm at *x*=1.5 mol.%. The increased grain size by doping MnO in NBT-based ceramics has also been observed in our previous research [26, 34].

The dielectric constant (ε_r) and dielectric loss tangent (tanδ) as a function of temperature for NBT-ST-*x*Mn ceramics measured at 1, 10 and 100 kHz are displayed in Fig.3 (a)-(d). As ε_r-*T* curves shown, one distinctive dielectric anomaly with a strong frequency-dependent dispersion at a lower temperature and a relatively weak frequency-dependent dispersion at a higher temperature are observed for all the

samples. One distinctive dielectric anomaly observed in ε_r-T curves proved that the phase structure is the T phase at room temperature, which is in accordance with the XRD analysis. The temperature at which the ε_r reaches its maximum value is assigned to the curie temperature T_m, which corresponds to the phase transition from the relaxation phase to the paraelectric phase [35]. With x increasing, the T_m (1kHz) increases obviously while the maximum value of ε_r enhances firstly and then have some decrease, as shown in Fig.3 (e). The enhanced T_m is beneficial for the temperature stability of strains. Moreover, all the samples exhibit broadness peaks at T_m, suggesting a relaxor behavior in these ceramics.

For relaxor ferroelectrics, the diffuseness in the phase transition can be described by the following equation [36]

$$1/\varepsilon_r - 1/\varepsilon_{max} = C^{-\gamma}(T - T_{max}) \quad (1)$$

where C is the Curie-like coefficient and γ is the degree of relaxation ranging between 1 for a normal ferroelectric and 2 for an ideal relaxor ferroelectric. The plots of $\ln(1/\varepsilon_r - 1/\varepsilon_{max})$ versus $\ln(T - T_{max})$ for NBT-ST-xMn ceramics are shown in Fig. 3 (f). According to the equation (1), the calculated values of γ have an obvious increase after doping MnO. The increase of γ is attributed to that the adding of Mn^{2+} ions (0.067 nm) would occupy Ti^{4+}(0.0605nm) sites due to the similarity in ionic radius, which means the B position is occupied by two kinds of ions after doping MnO. Accordingly, the composition and structure of NBT-ST-xMn ceramics is inevitably to be fluctuated, leading to the increase of γ values. Schütz et al. [37] reported that relaxor behavior would be conducive to trigger a giant strain. Thus, the increase of γ values induced by the addition of Mn ions may be beneficial to obtain large strain.

Fig. 4 exhibits the bipolar P-E hysteresis loops and S-E curves of NBT-ST-xMn ceramics measured at 10 Hz under an electric feld of 60 kV/cm. Comparing with unmodified 0.65NBT-0.35ST ceramic, the maximum polarization (P_{max}) enhances obviously while the remanent polarization (P_r) and coercive field (E_c) decrease in varying extent after doping MnO. The P_{max} value can be enhanced to 34 μC/cm^2 while the P_r value is only 2.8 μC/cm^2 under 60 kV/cm at x=1.0 mol.%. The obviously decrease of P_r clearly demonstrated that the defect dipoles also exist in Mn-doped

0.65NBT-0.35ST ceramics. The associated defect dipole moment (P_D) can act as an internal field to switch the new domain back to its original state after removing the electric field, leading to the pinched and double *P-E* hysteresis loops with large P_{max} and small P_r [38,39]. As the *S-E* curves shown, there is almost no negative strain can be seen for all the samples, which is the typical piezoelectric response for relaxor ferroelectric materials.

From the application point of view, low hysteresis (*H*) is as important as strain values. The strain values *S* and hysteresis *H* ($H=\triangle S/S_{max}$, $\triangle S$ and S_{max} are measured at $E_{max}/2$ and E_{max}, respectively) as a function of doping content for NBT-ST-*x*Mn ceramics are displayed in Fig.5. With the increase of MnO doping, the strain increases firstly and then has a slight decrease while the hysteresis decreases firstly and then has some increase. The maximum value of strain can be up to 0.22% at 60 kV/cm with ultra-low hysteresis of 14% when 1.0 mol.% MnO is doped. The improvement of strain values for NBT-ST-*x*Mn ceramics is attributed to the introduction of defect dipoles, the enhancement of relaxor behavior and the increased grain size [13, 40]. This result illustrates that the appropriate addition of MnO in 0.65NBT-0.35ST ceramic could not only enhance the maximum achievable strain value but also decrease the hysteresis.

In order to clearly compare the actuation properties of NBT-based materials, data from previous literatures that devoted to reduce the hysteresis are listed in Table 1. Obviously, the hysteresis of NBT-based ceramics is still more than 20% by doping with effective chemical modifiers or designing ceramic/ceramic composites, and small hysteresis (10-20%) could be obtained only by optimizing the preceding techniques, such as texture control or using spark plasma sintering (SPS) method. Here, a relatively high strain of 0.22% with ultra-low hysteresis of 14% are achieved simultaneously at 60 kV/cm by doping MnO into 0.65-NBT-0.35ST ceramics. The result illustrates that the proper selection of base composition and effective chemical modifier can obtain large strain under low electric field meanwhile maintain ultra-low hysteresis.

Table 1 Comparison of electro-strain S, strain hysteresis H and E_{max} values of NBT-based ceramics

Material	S (%)	H (%)	E_{max} (kV/cm)	Ref.
NBT-KBT-BST-2%Nb	0.38	40	60	[23]
NBT-KBT-2%BZT	0.32	40	65	[24]
NBT-KBT-6%SBZT	0.72	36	110	[25]
0.70NBT-0.30ST-0.5%Mn	0.32	28	60	[26]
NBT-KBT-2%BCZ	0.30	25	55	[27]
BNT-BT-10KNN	0.16	25	80	[31]
NBT-KBT-4%BA	0.21	24	70	[32]
NBT-KBT- $Bi_4Ti_3O_{12}$	0.29	23	60	[33]
NBT-BT-ST-1.1%Mn	0.24	10	80	[34]
BNT-BT-2.5%LN (SPS)	0.64	19.5	50	[17]
Textured KBT-BT-NBT	0.48	17	130	[41]
0.65NBT-0.35ST-1.0%Mn	0.22	14	60	This work

Large strain with ultra-low hysteresis is beneficial to obtain purely electrostrictive effect. Fig. 6 presents the S-P^2 plots derived from the corresponding polarization and strain hysteresis loops of NBT-ST-xMn ceramics. The electrostrictive effect can be calculated by the formula: $S=Q_{33}P^2$, where S, Q_{33}, and P are the strain, electrostrictive coefficient, and polarization, respectively [26]. The hysteresis has made the S-P^2 curve deviate slightly from a quadratic relationship at x=0.0% and x=1.5%. For 0.5 % and 1.0 % Mn-doped ceramics, a pretty linear dependence of strain on polarization square can be noted, classifying that "purely" electrostrictive effects are achieved. The calculated Q_{33} value for 0.5 % Mn-doped NBT-ST ceramic is 0.022 m^4/C^2, which is no smaller than that of the representative electrostrictive materials in the literature [24, 26, 31, 34].

Except for the high strain with ultra-low hysteresis, Mn doping also contribute to enhance the energy storage density of 0.65NBT-0.35ST ceramics. Generally, energy-storage density of nonlinear dielectric ceramics can be calculated by the unipolar P-E loop with the following equations: [42]

$$W_{\text{rec}} = \int_{P_r}^{P_{\max}} EdP \tag{2}$$

$$\eta = \frac{W_{\text{rec}}}{W_{\text{rec}} + W_{\text{loss}}} \times 100\% \tag{3}$$

where W_{rec}, W_{loss} and η denote the recoverable energy storage density, energy loss density and energy storage efficiency, respectively. It can be seen from the above equations that large $P_{\max}$, small P_{r} and high BDS is very important to achieve high energy storage density. In order to investigate the electric-field-strength dependence on the energy storage, the unipolar *P-E* loops of the NBT-ST-*x*Mn ceramics samples measured in the electric field ranging from 10 to 70 kVcm^{-1} at room temperature are shown in Fig.7. Similar to the bipolar *P-E* loops, the obtained unipolar *P-E* loops become slimmer after doping with MnO. Additionally, compared with the unmodified 0.65NBT-0.35ST ceramic, the $P_{\max}$ increases significantly while P_{r} decreases in varying extent, and the Mn-doped samples always maintain low P_{r} with different electric fields due to the introduction of defect dipoles. Thus, the energy storage properties of NBT-based ceramics could be improved by the addition of MnO.

Based on equations (2)-(3) and obtained unipolar *P-E* loops of Fig.7(a)-(d), the calculated W_{rec}, W_{loss} and η of the NBT-ST-*x*Mn ceramics are presented in Fig.8. The W_{rec} and W_{loss} of all the samples increase by different degrees with increasing applied electric field. Noteworthily, after introducing MnO into the 0.65NBT-0.35ST ceramic, the W_{rec} values improve obviously due to the enhanced $P_{\max}$ and reduced P_{r}. The maximum W_{rec} value for the NBT-ST-*x*Mn ceramics increase to as high as 0.92 J cm^{-3} at 70 kV/cm for *x*=1.0 mol.%. Meanwhile, the W_{loss} values of Mn-doped samples decrease to some certain degree at high electric field due to the result that shape of *P-E* loops changes from fat to pinched, leading to the enhancement of η (shown in the inset of Fig.8 (a)). The η values increase from 64% for *x*=0.0 mol.% to 81%, 78% and 73% at *x*=0.5, 1.0 and 1.5 mol.%, respectively. These results illustrate that the addition of MnO could boost the energy storage property of 0.65NBT-0.35ST solid solution effectively.

In addition, the BDS is also a very important parameter for energy storage ceramics. Thus, the BDS of NBT-ST-*x*Mn ceramics was also analyzed by Weibull

distribution [26,43], as shown in Fig. 9(a). The average BDS is determined by fitting lines and the results are displayed in the inset of Fig. 9(a). It can be found that all the samples fit well with the Weibull distribution function. The BDS of NBT-ST-*x*Mn ceramics can be enhanced with MnO doping, and the BDS values are 74, 89, 83 and 80 kV/cm for 0.0-1.5 mol.‰ Mn-doped ceramics, respectively. Previous researches revealed that the addition of 'hard' dopant (Fe, Mn, etc.) is believed to be an effective method to improve BDS [44,45].The enhancement of BDS for NBT-ST-*x*Mn ceramics may be caused by the 'hard' dopant. Fig. 9(b) presents unipolar *P-E* loops of the NBT-ST-*x*Mn ceramics measured at their critical BDS. Clearly, large P_{max} and small P_r can be obtained simultaneously after doping MnO into 0.65NBT-0.35ST ceramic. The difference between P_{max} and P_r (P_{max}- P_r) of the four samples are displayed in Fig. 9(c). It can be found that the P_{max}-P_r value significantly enhanced by doping MnO, and the values can be up to 35 and 37 μC cm^{-2} at x=0.5 and 1.0 mol.%, respectively. Such high P_{max}-P_r and BDS values are beneficial for obtaining high energy storage density and efficiency. Fig. 9(d) presents the calculated W_{rec}, W_{loss} and η of the NBT-ST-*x*Mn ceramics. As expected, excellent energy storage performance of 1.14 and 1.17 J cm^{-3} with a high η of 83 and 80% are achieved at x=0.5 and 1.0 mol.%, respectively. The obtained results indicate that with proper doping of MnO into the NBT-ST ceramics, high W_{rec} and η can be achieved simultaneously due to the enhanced BDS and P_{max}-P_r value.

4 Conclusions

In conclusion, NBT-ST-*x*Mn lead-free ceramics were designed and prepared by solid state synthesis method. It has been found that the addition of MnO also can induce defect dipoles into 0.65NBT-0.35ST ceramic, which result in double *P-E* hysteresis loops with high P_{max} and small P_r. Accordingly, a relatively high strain of 0.22% with ultra-low hysteresis of 14% was achieved under a moderate electric field of 60 kV/cm at x=1.0 mol.% due to the introduction of defect dipoles, the enhancement of relaxor behavior and the increased grain size. Excellent energy storage performance of 1.14 and 1.17 J cm^{-3} with a high η of 83 and 80% were also

achieved at x=0.5 and 1.0 mol.% due to the enhanced BDS and P_{max}-P_r value. Meanwhile, high electrostriction coeffcient of 0.022 m^4C^2 with pure electrostrictive characteristics was obtained at x=0.5 mol.%. The findings demonstrate that MnO-doped NBT-based ceramics are promising to be applicable for actuators and energy storage devices.

Acknowledgement

This work was supported by the National Natural Science Foundation of China (No. 51802061, 51677033 and 51702069), University Nursing Program for Young Scholars with Creative Talents in Heilongjiang Province (No. UNPYSCT-2020215), Youth Innovative Talent Support Program of Harbin University of Commerce (No. 2020CX05), and Doctoral Start-up Scientific Research Foundation of Harbin University of Commerce (No. 2019DS078).

References

[1] Gubinyi Z, Batur C, Sayir A, *et al*. Electrical properties of PZT piezoelectric ceramics at high temperatures. *J Electroceram* 2007, **20**: 95-105.

[2] Chen JG, Shi HD, Liu GX, *et al*. Temperature dependence of dielectric, piezoelectric and elastic properties of $BiScO_3$-$PbTiO_3$ high temperature ceramics with morphotropic phase boundary (MPB) composition. *J Alloys Compd* 2012, **537**: 280-285.

[3] Li F, Jin L, Xu Z, *et al*. Electrostrictive effect in $Pb(Mg_{1/3}Nb_{2/3})O_3$-$x$$PbTiO_3$ crystals. *Appl Phys Lett* 2013, **102**: 152910.

[4] Jia WX, Hou YD, Zheng MP, *et al*. Advances in lead-free high-temperature dielectric materials for ceramic capacitor application. *IET Nanodielectr* 2018, **1**: 3-16.

[5] Li DX, Shen ZY, Li ZP, *et al*. P-E hysteresis loop going slim in $Ba_{0.3}Sr_{0.7}TiO_3$-modified $Bi_{0.5}Na_{0.5}TiO_3$ ceramics for energy storage applications. *J Adv Ceram* 2020, **9**(2): 183–192.

[6] Jia H, Hu XK, Chen JG. Temperature-dependent piezoelectric strain and resonance performance of Fe_2O_3-modified $BiScO_3$-$PbTiO_3$-$Pb(Nb_{1/3}Mn_{2/3})O_3$ ceramics. *J Eur Ceram Soc* 2019, **39**: 2348-2353.

[7] Xie H, Yang L, Pang SJ, *et al*.The evolution of phase structure, dielectric, strain, and energy storage density of complex-ions $(Sr_{1/3}Nb_{2/3})^{4+}$ doped $0.82Bi_{0.5}Na_{0.5}TiO_3$-$0.18Bi_{0.5}K_{0.5}TiO_3$ ceramics. *J Phys Chem Solid* 2019, **126**: 287–293.

[8] Wang HX, Zhao PY, Chen LL, *et al*. Energy storage properties of $0.87BaTiO_3$-$0.13Bi(Zn_{2/3}(Nb_{0.85}Ta_{0.15})_{1/3})O_3$ multilayer ceramic capacitors with thin dielectric layers. *J Adv Ceram* 2020, **9**(3): 292–302.

[9] Habib M, Munir M, Khan SA, *et al*. Evaluation of high strain response in lead-free BNBTFS-xNb ceramics by structure and ferroelectric characterizations. *J Phys Chem Solid* 2020, **138**: 109230.

[10] Zhang ST, Kounga AB, Aulbach E, *et al*. Giant strain in lead-free piezoceramics $Bi_{0.5}Na_{0.5}TiO_3$-$BaTiO_3$-$K_{0.5}Na_{0.5}NbO_3$ system. *Appl Phys Lett* 2007, **91**(11): 112906.

[11] Hiruma Y, Imai Y, Watanabe Y, *et al*. Large electrostrain near the phase transition temperature of $(Bi_{0.5}Na_{0.5})TiO_3$-$SrTiO_3$ ferroelectric ceramics. *Appl Phys Lett* 2008, **92**: 262904.

[12] Jo W, Granzow T, Aulbach E, *et al*. Origin of the large strain response in $(K_{0.5}Na_{0.5})NbO_3$-modified $(Bi_{0.5}Na_{0.5})TiO_3$-$BaTiO_3$ lead-free piezoceramics. *J Appl Phys* 2009, **105**: 094102.

[13] Liu XM, Tan XL. Giant strains in non-textured $(Bi_{1/2}Na_{1/2})TiO_3$-based lead-free ceramics. *Adv Mater* 2016, **28**: 574-578.

[14] Hao J, Xu Z, Chu R, *et al*. Field-induced large strain in lead-free $(Bi_{0.5}Na_{0.5})_{1-x}Ba_xTi_{0.98}(Fe_{0.5}Ta_{0.5})_{0.02}O_3$ piezoelectric ceramics. *J Alloy Comp* 2016, **677**: 96-104.

[15] Wang C, Li Q, Yadav AK, *et al*. $Bi_{0.48}(Na_{0.84}K_{0.16})_{0.48}Sr_{0.04}(Ti_{1-x}Ta_x)O_3$ lead-free ceramics with enhanced electric field-induced strain. *J Alloy Comp* 2019, **803**: 1082-1089.

[16] Zhang HB, Ma WG, Xie B, *et al*. $(Na_{1/2}Bi_{1/2})TiO_3$-based lead-free co-fired multilayer actuators with large strain and high fatigue resistance. *J Am Ceram Soc* 2019, **102**: 6147-6155.

[17] Chen J, Wang YP, Wu L, *et al*. Effect of nanocrystalline structures on the large strain of $LiNbO_3$ doped $(Bi_{0.5}Na_{0.5})TiO_3$-$BaTiO_3$ materials. *J Alloys Comp* 2019, **775**: 865-871.

[18] Si Y, Li Y, Li L, *et al*. Giant electro-strain in textured Li^+-doped 0.852BNT-0.11BKT-0.038BT ternary lead-free piezoelectric ceramics. *J Am Ceram Soc* 2019, **00**: 1-8.

[19] Gong YY, He X, Chen C, *et al*. Large electric field-induced strain in ternary $Bi_{0.5}Na_{0.5}TiO_3$-$BaTiO_3$-Sr_2MnSbO_6 lead-free ceramics. *Ceram Int* 2019, **45**: 7173-7179.

[20] Liu X, Xue SD, Wang FF, *et al*. Grain size dependent physical properties in lead-free

multifunctional piezoceramics: A case study of NBT-*x*ST system. *Acta Mater* 2019, **164**: 12-24.

[21] Li L, Zhang J, Wang RX, *et al*. Thermally-stable large strain in $Bi(Mn_{0.5}Ti_{0.5})O_3$ modifed $0.8Bi_{0.5}Na_{0.5}TiO_3$-$0.2Bi_{0.5}K_{0.5}TiO_3$ ceramics. *J Eur Ceram Soc* 2019, **39**: 1827-1836.

[22] Manotham S, Jaita P, Randorn C, *et al*. Excellent electric field-induced strain with high electrostrictive and energy storage performance properties observed in lead-free $Bi_{0.5}(Na_{0.84}K_{0.16})_{0.5}TiO_3$-$Ba(Nb_{0.01}Ti_{0.99})O_3$-$BiFeO_3$ ceramics. *J Alloy Comp* 2019, **808**: 151655.

[23] Ullah A, Malik RA, Ullah A, *et al*. Electric-field-induced phase transition and large strain in lead-free Nb-doped BNKT-BST ceramics. *J Eur Ceram Soc* 2014, **34**: 29-35.

[24] Bai WF, Chen DQ, Huang YW, *et al*. Temperature-insensitive large strain response with a low hysteresis behavior in NBT-based ceramics. *Ceram Int* 2016, **42**: 7669-7680.

[25] Li TY, Lou XJ, Ke XQ, *et al*. Giant strain with low hysteresis in A-site-deficient $(Bi_{0.5}Na_{0.5})TiO_3$-based lead-free piezoceramics. *Acta Mater* 2017, **128**: 337-344.

[26] Cao WP, Sheng J, Qiao YL, *et al*. Optimized strain with small hysteresis and high energy-storage density in Mn-doped NBT-ST system. J. Eur. Ceram. Soc. 39 (2019) 4046-4052.

[27] Lee HB, Heo DJ, Malik RA, *et al*. Lead-free $Bi_{1/2}(Na_{0.82}K_{0.18})_{1/2}TiO_3$ ceramics exhibiting large strain with small hysteresis. *Ceram Int* 2013, 39: S705-S708.

[28] Khansur NH, Groh C, Jo W, *et al*. Tailoring of unipolar strain in lead-free piezoelectrics using the ceramic/ceramic composite approach. *J Appl Phys* 2014, **115**: 124108.

[29] Groh C, Franzbach DJ, Jo W, *et al*. Relaxor/ferroelectric composites: a solution in the quest for practically viable lead-free incipient piezoceramics. *Adv Funct Mater* 2014, **24**: 356-362.

[30] Zhang H, Groh C, Zhang Q, *et al*. Large strain in relaxor/ferroelectric composite lead-free piezoceramics. *Adv Electron Mater* 2015, **1**: 1500018.

[31] Zhang ST, Kounga AB, Jo W, *et al*. High-strain lead-free antiferroelectric electrostrictors. *Adv Mater* 2009, **21**: 4716-4721.

[32] Qian H, Yu ZL, Mao MM, *et al*. Nanoscale origins of small hysteresis and remnant strain in $Bi_{0.5}Na_{0.5}TiO_3$-based lead-free ceramics. *J Eur Ceram Soc* 2017, 37: 3483-3491.

[33] Fan PY, Zhang YY, Zhang Q, *et al*. Large strain with low hysteresis in $Bi_4Ti_3O_{12}$ modified $Bi_{1/2}(Na_{0.82}K_{0.18})_{1/2}TiO_3$ lead-free piezoceramics. *J Eur Ceram Soc* 2018, **38**: 4404-4413.

[34] Cao WP, Li WL, Feng Y, *et al*. Defect dipole induced large recoverable strain and high energy-storage density in lead free $Na_{0.5}Bi_{0.5}TiO_3$-based systems. *Appl Phys Lett* 2016, **108**:

202902.

[35] Cao WP, Li WL, Dai XF, *et al*. Large electrocaloric response and high energy-storage properties over a broad temperature range in lead-free NBT-ST ceramics. *J Eur Ceram Soc* 2016, **36**: 593-600.

[36] Malathi AR, Devi CS, Kumar GS, *et al*. Dielectric relaxation in NBT-ST ceramic composite materials. *Ionics* 2013, **19**: 1751-1760.

[37] Schütz D, Deluca M, Krauss W, *et al*. Lone-Pair-Induced Covalency as the Cause of Temperature- and Field-Induced Instabilities in Bismuth Sodium Titanate. *Adv Funct Mater* 2012, **22**: 2285-2294.

[38] Feng ZY, Ren X. Aging effect and large recoverable electrostrain in Mn-doped $KNbO_3$-based ferroelectrics. *Appl Phys Lett* 2007, **91**: 032904.

[39] Zhang LX, Chen W, Ren X. Large recoverable electrostrain in Mn-doped (Ba,Sr)TiO_3 ceramics. Appl Phys Lett 85 (2004) 5658-5660.

[40] Li HL, Liu Q, Zhou JJ, *et al*. Grain size dependent electrostrain in $Bi_{1/2}Na_{1/2}TiO_3$-$SrTiO_3$ incipient piezoceramics. *J Eur Ceram Soc* 2016, **36**: 2849-2853.

[41] Maurya D, Zhou Y, Wang Y, *et al*. Giant strain with ultra-low hysteresis and high temperature stability in grain oriented lead-free $K_{0.5}Bi_{0.5}TiO_3$-$BaTiO_3$-$Na_{0.5}Bi_{0.5}TiO_3$ piezoelectric materials. *Sci Rep* 2015, **5**: 85-95.

[42] Yan F, Huang KW, Jiang T, *et al*. Significantly enhanced energy storage density and efficiency of BNT-based perovskite ceramics via A-site defect engineering. Energy Storage Mater 2020, **30**: 392-400.

[43] Jain A, Wang YG, Guo H. Microstructure induced ultra-high energy storage density coupled with rapid discharge properties in lead-free $Ba_{0.9}Ca_{0.1}Ti_{0.9}Zr_{0.1}O_3$-$SrNb_2O_6$ ceramics. *Ceram Int* 2021, **47**: 487-499.

[44] Li F, Zhai J, Shen B, *et al*. Simultaneously high-energy storage density and responsivity in quasi-hysteresis-free Mn-doped $Bi_{0.5}Na_{0.5}TiO_3$-$BaTiO_3$-$(Sr_{0.7}Bi_{0.2}\square_{0.1})TiO_3$ ergodic relaxor ceramics. *Mater Res Lett* 2018, **6**: 345-352.

[45] Qu B, Du H, Yang Z. Lead-free relaxor ferroelectric ceramics with high optical transparency and energy storage ability. *J Mater Chem C* 2016, **4**: 1795-1803.

Captures

Fig.1 X-ray diffraction patterns of NBT-ST-*x*Mn ceramics (a) 20-80°, (b) 45-48°

Fig.2 Surface morphologies of NBT-ST-*x*Mn ceramics (a) *x*=0.0 %, (b) *x*=0.5 %, (c) *x*=1.0 %, (d) *x*=1.5 %

Fig.3 (a)-(d) Temperature dependent of dielectric constant and dielectric loss, (e) T_m value and the maximum value of ε_r and (f) plots of $\ln(1/\varepsilon_r-1/\varepsilon_{max})$ versus $\ln(T-T_{max})$ of NBT-ST-*x*Mn ceramics

Fig.4 Electric-field-induced polarization and strain of NBT-ST-*x*Mn ceramics (a) *x*=0.0 %, (b) *x*=0.5 %, (c) *x*=1.0 %, (d) *x*=1.5 %

Fig.5 Strain values and strain hysteresis as a function of doping content for NBT-ST-*x*Mn ceramics

Fig.6 Strain as function of P^2 of NBT-ST-*x*Mn ceramics (a) *x*=0.0 %, (b) *x*=0.5 %, (c) *x*=1.0 %, (d) *x*=1.5 %

Fig. 7 The unipolar *P-E* loop as a function of electric field for NBT-ST-*x*Mn ceramics (a) *x*=0.0 %, (b) *x*=0.5 %, (c) *x*=1.0 %, (d) *x*=1.5 %

Fig. 8 Energy storage performance of NBT-ST-*x*Mn ceramics under different electric fields (a) recoverable energy density W_{rec}, (b) the energy loss density W_{loss}. The the inset is energy storage efficiency η

Fig. 9 (a) Weibull distribution and the fitting lines of BDS (b) unipolar *P-E* loops measured at their critical BDS (c) variation of P_{max}-P_r value and (d) W_{rec}, W_{loss} and η of NBT-ST-*x*Mn ceramics

Figures

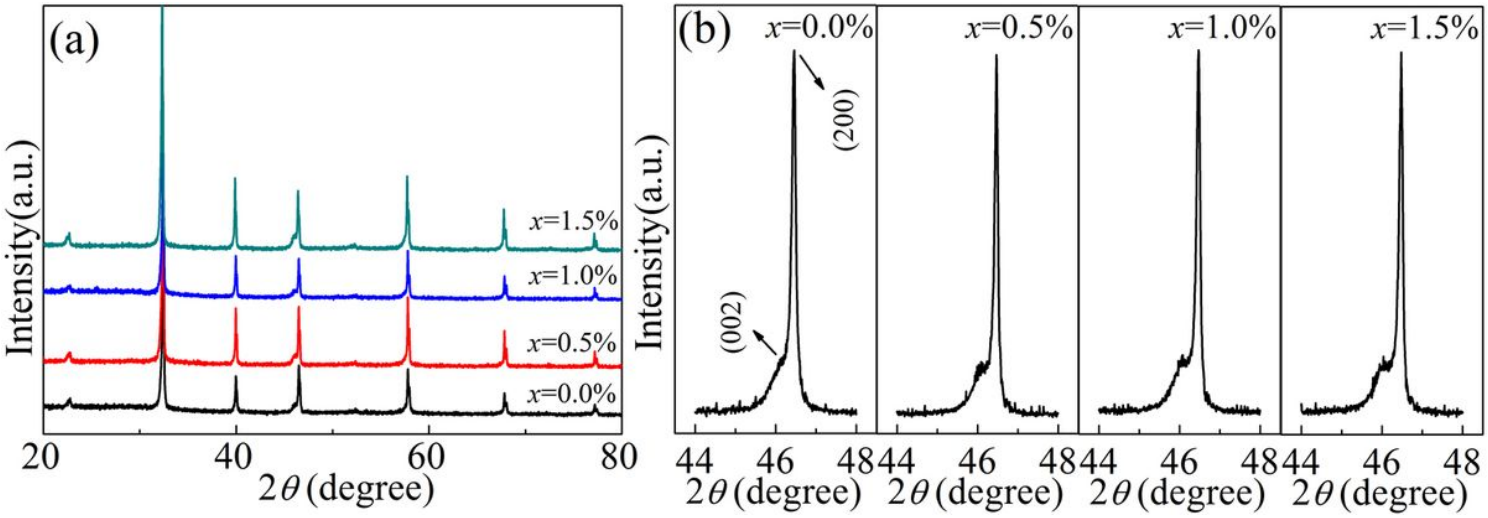

Figure 1

X-ray diffraction patterns of NBT-ST-xMn ceramics (a) 20-80o, (b) 45-48o

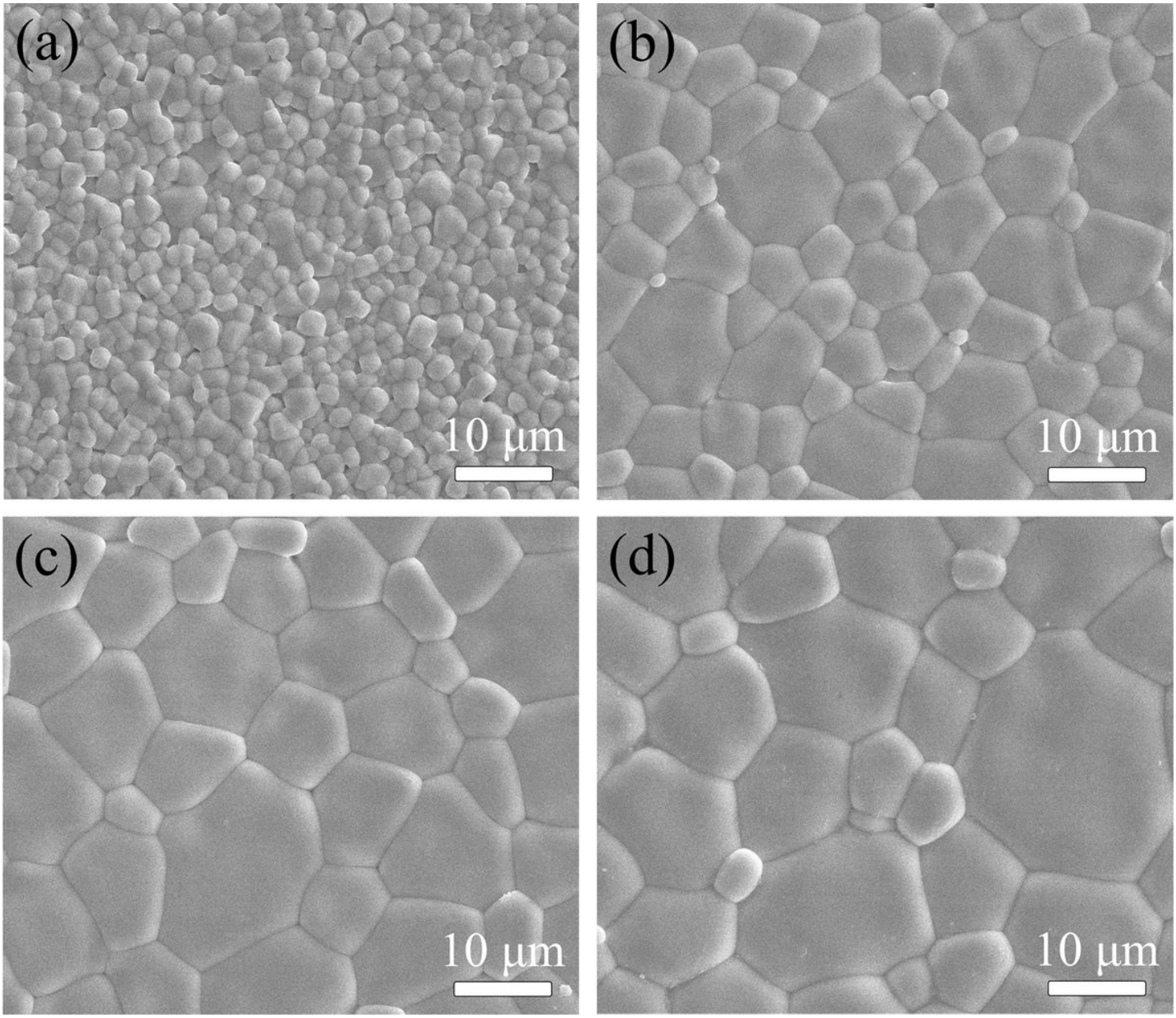

Figure 2

Surface morphologies of NBT-ST-xMn ceramics (a) x=0.0 %, (b) x=0.5 %, (c) x=1.0 %, (d) x=1.5 %

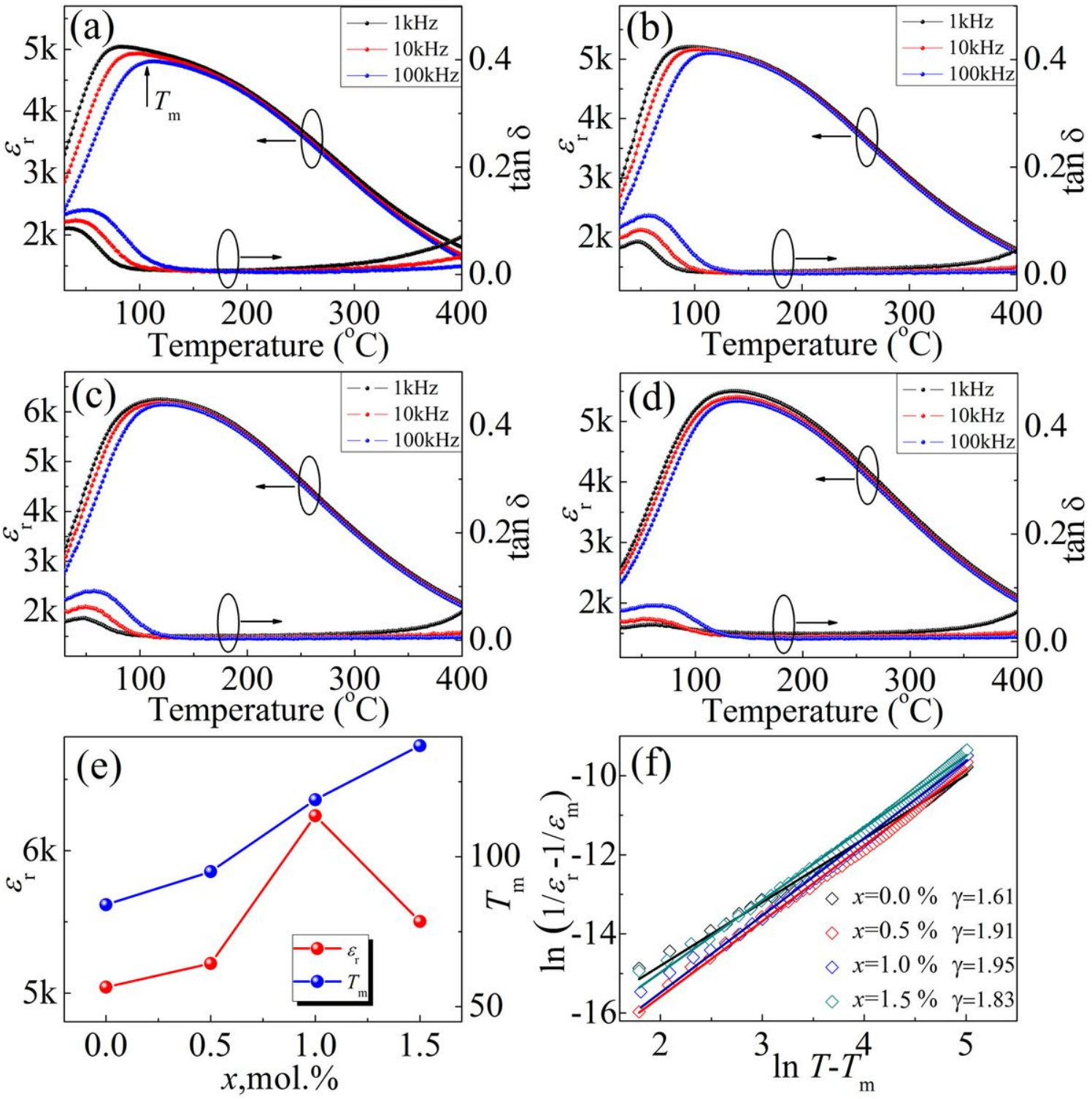

Figure 3

(a)-(d) Temperature dependent of dielectric constant and dielectric loss, (e) Tm value and the maximum value of εr and (f) plots of ln(1/εr-1/εmax) versus ln(T-Tmax) of NBT-ST-xMn ceramics

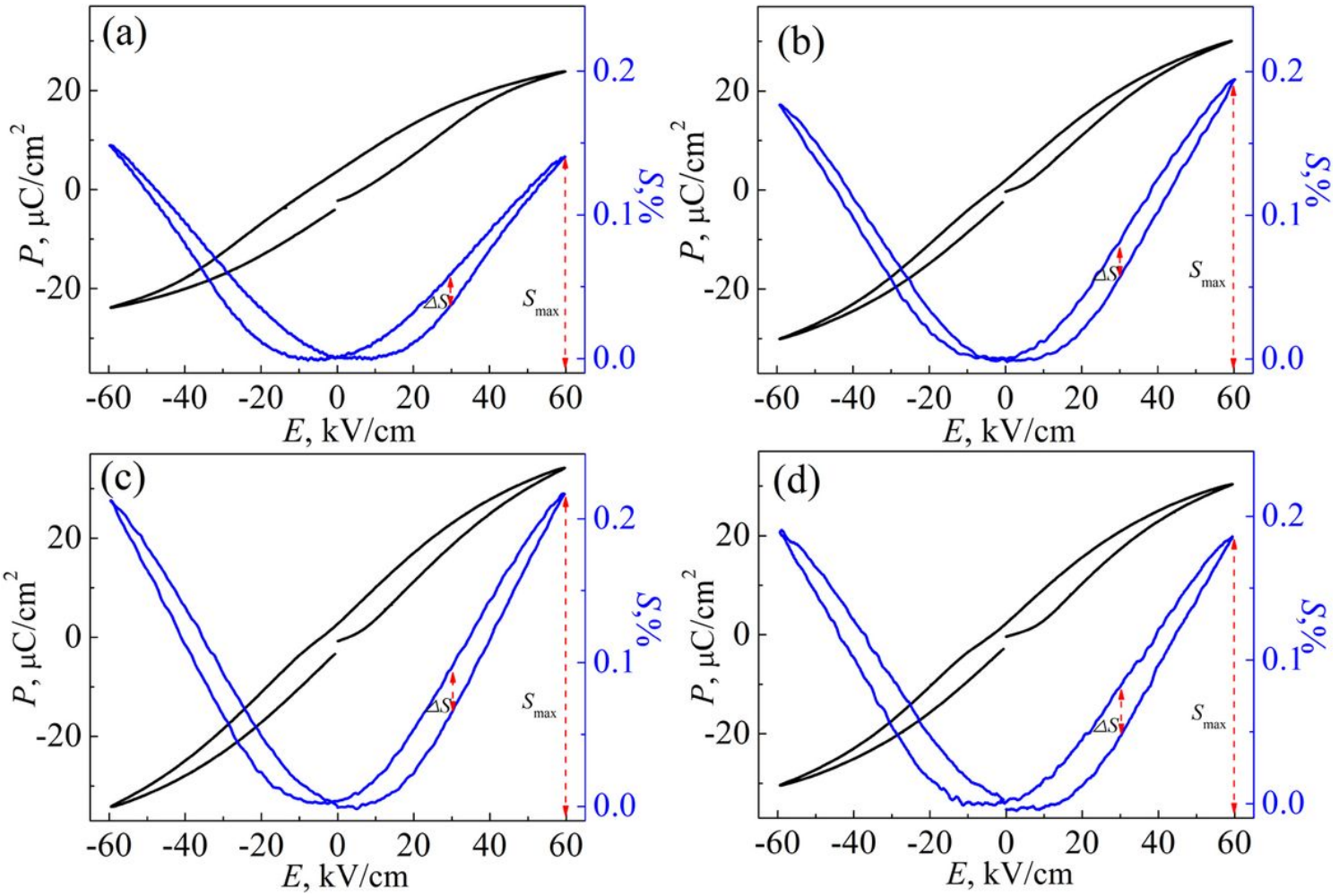

Figure 4

Electric-field-induced polarization and strain of NBT-ST-xMn ceramics (a) x=0.0 %, (b) x=0.5 %, (c) x=1.0 %, (d) x=1.5 %

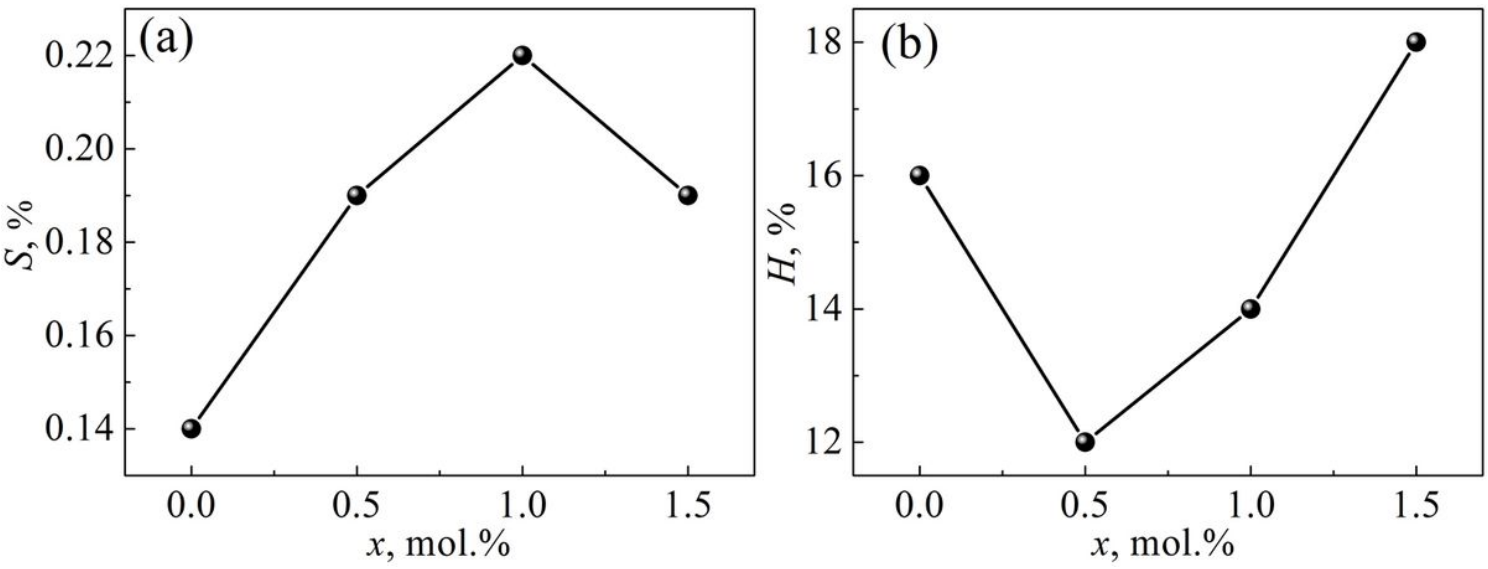

Figure 5

Strain values and strain hysteresis as a function of doping content for NBT-ST-xMn ceramics

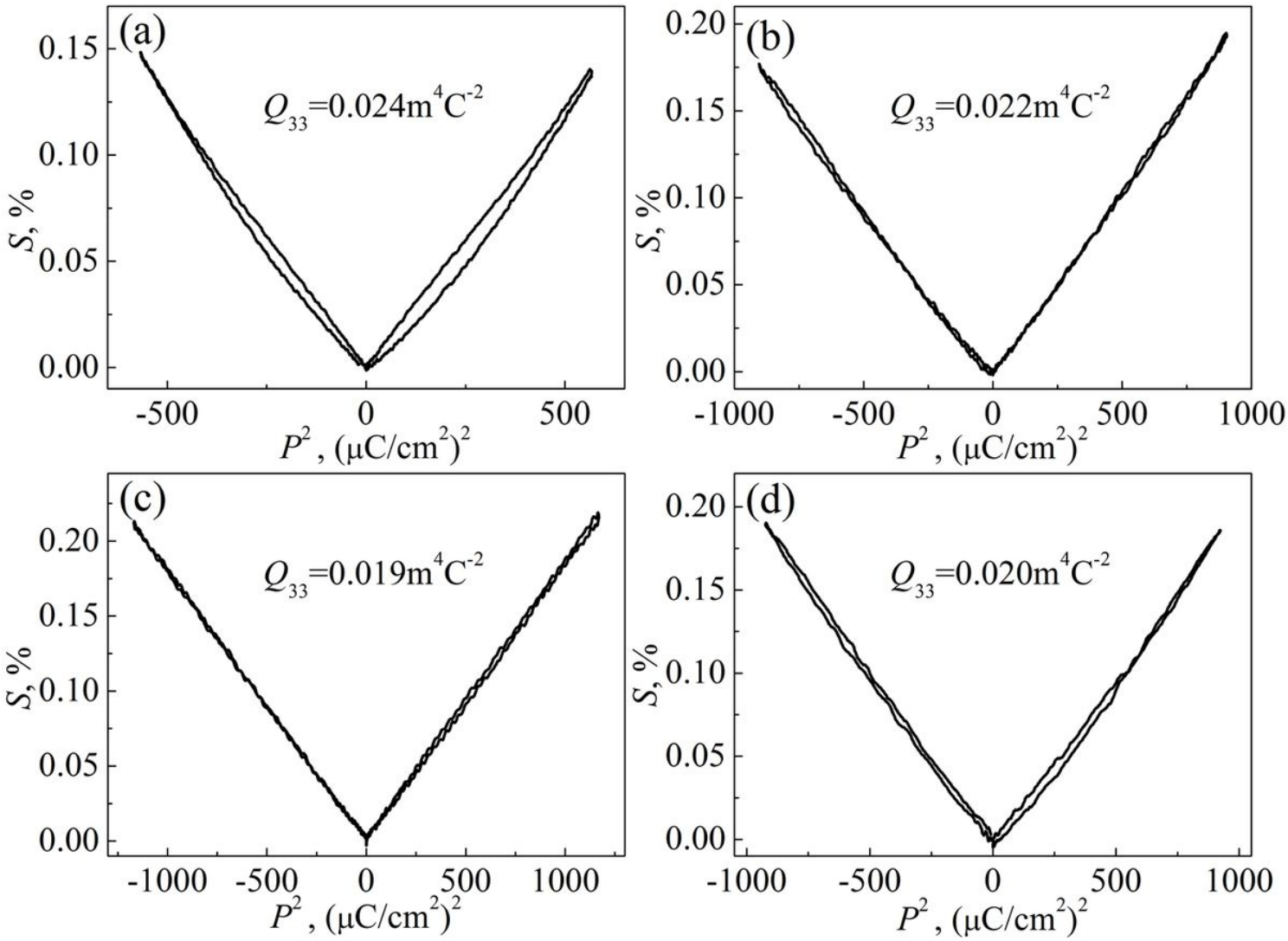

Figure 6

Strain as function of P2 of NBT-ST-xMn ceramics (a) x=0.0 %, (b) x=0.5 %, (c) x=1.0 %, (d) x=1.5 %

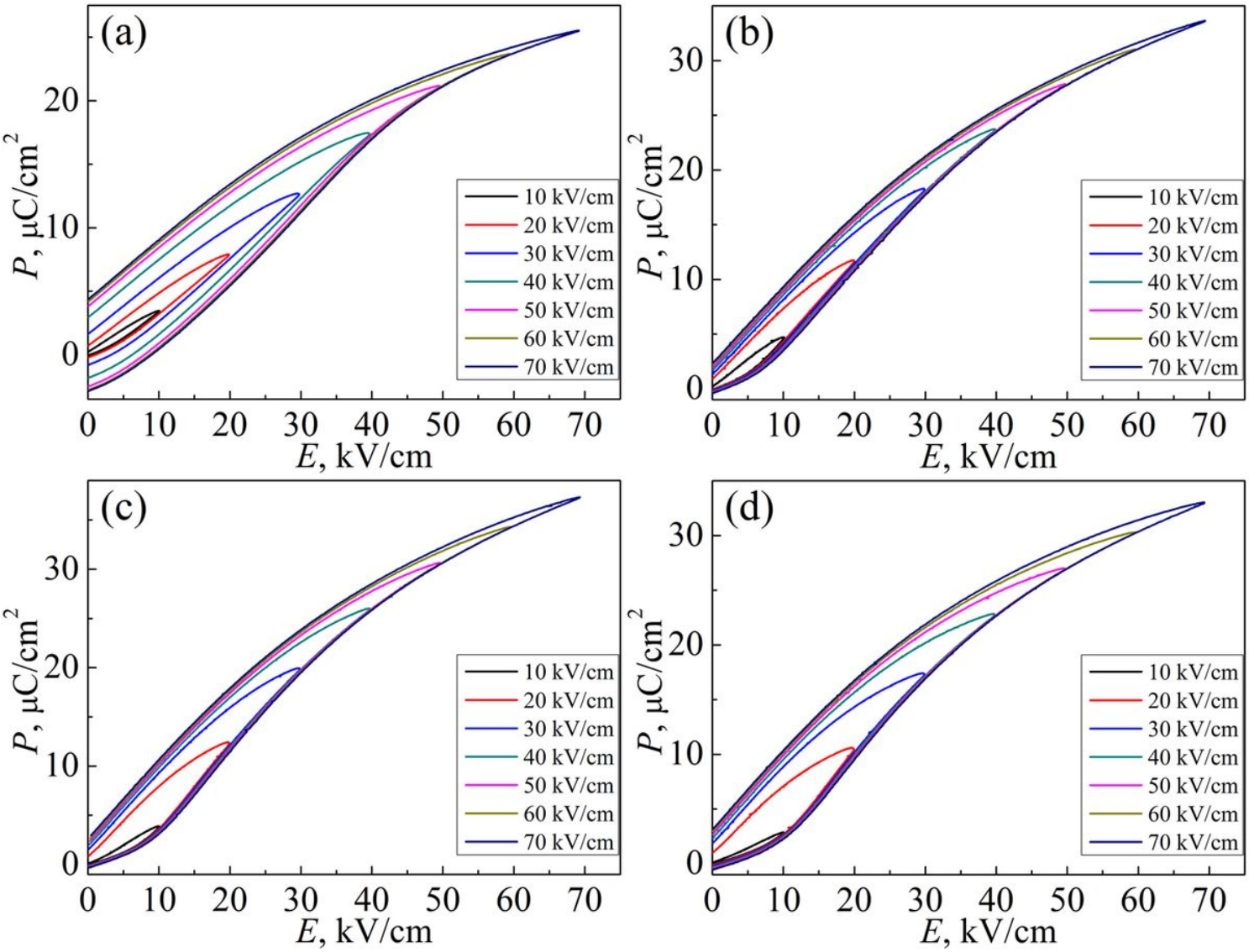

Figure 7

The unipolar P-E loop as a function of electric field for NBT-ST-xMn ceramics (a) x=0.0 %, (b) x=0.5 %, (c) x=1.0 %, (d) x=1.5 %

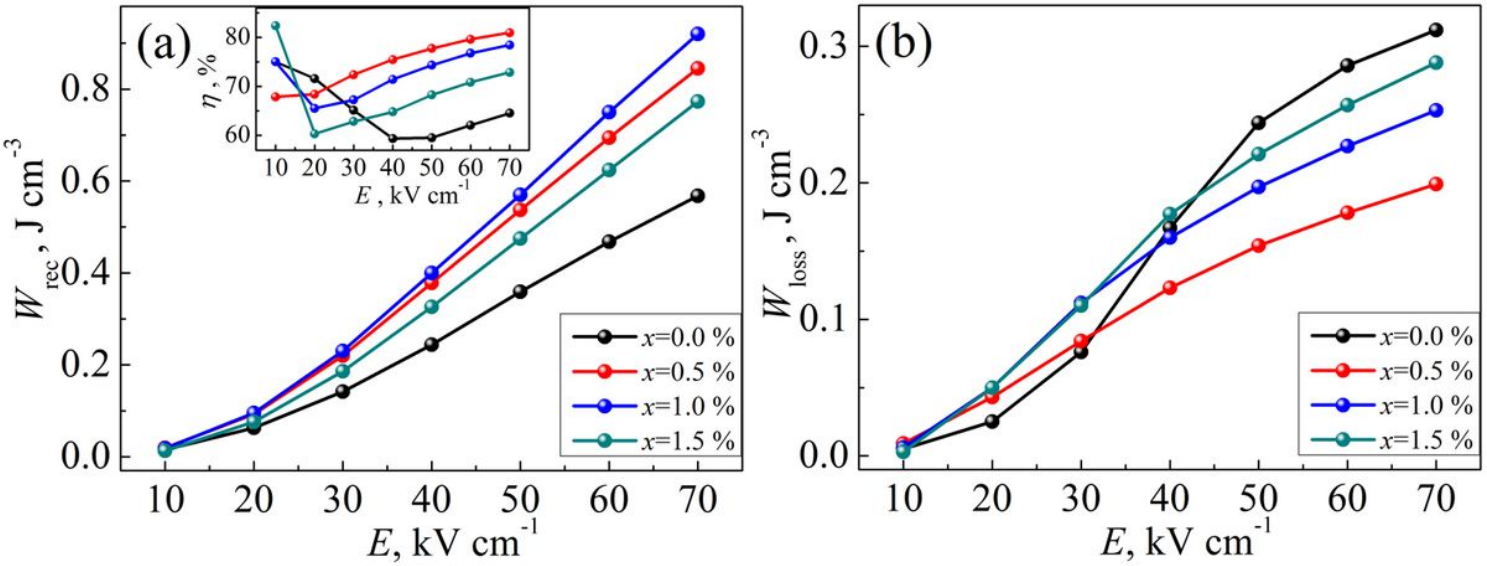

Figure 8

Energy storage performance of NBT-ST-xMn ceramics under different electric fields (a) recoverable energy density Wrec, (b) the energy loss density Wloss. The the inset is energy storage efficiency η

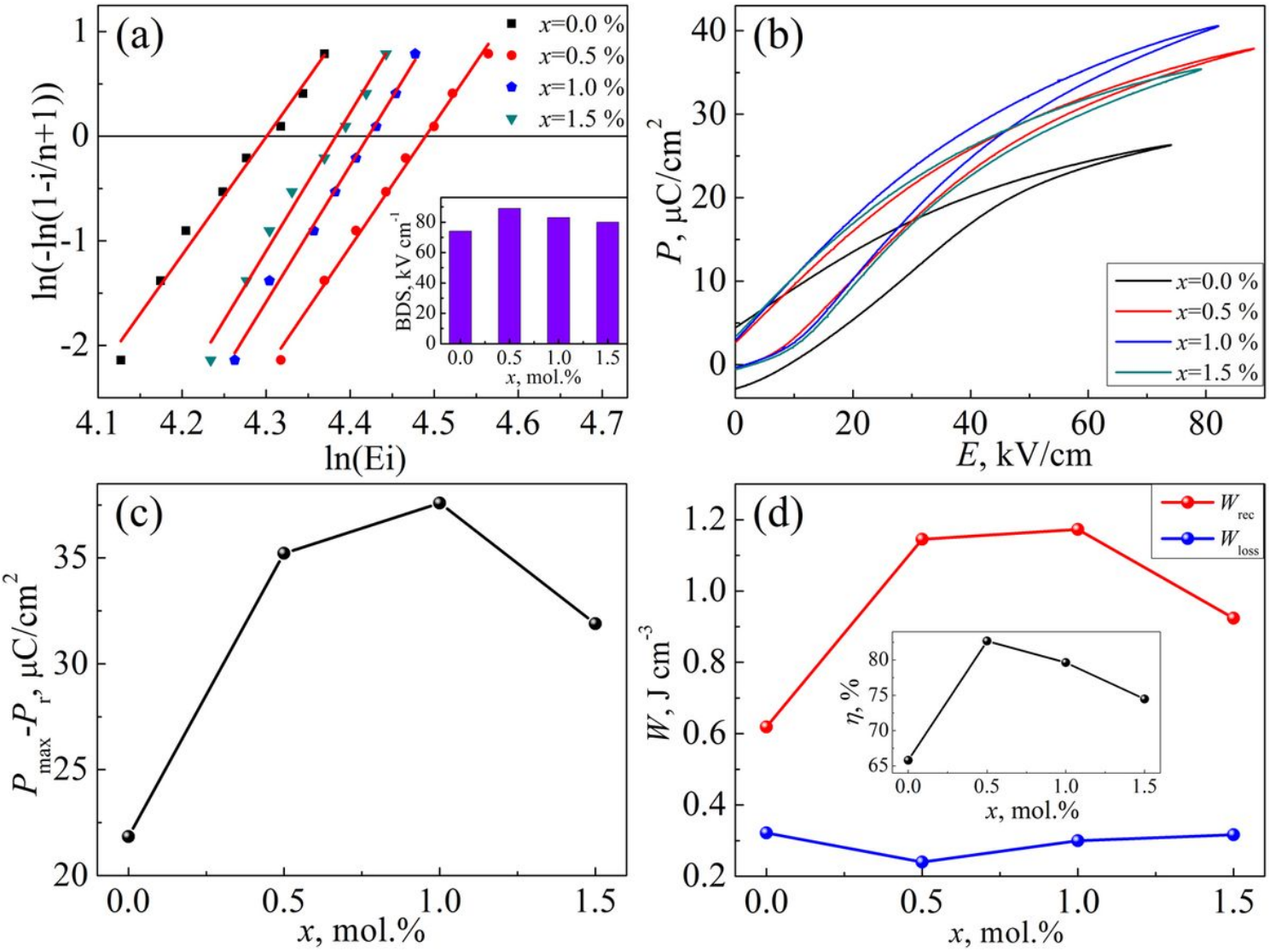

Figure 9

(a) Weibull distribution and the fitting lines of BDS (b) unipolar P-E loops measured at their critical BDS (c) variation of Pmax-Pr value and (d) Wrec, Wloss and η of NBT-ST-xMn ceramics